Bacteria Navigate Anisotropic Media using a Flagellar Tug-of-Oars

Ameya G. Prabhune ●,[1] Andy S. García-Gordillo ●,[1] Igor S. Aranson ●,[2]
Thomas R. Powers ●,[3] and Nuris Figueroa-Morales ●[1,*]

[1]*Department of Physics, University of Colorado Boulder, Boulder, Colorado 80309, USA*
[2]*Department of Biomedical Engineering, The Pennsylvania State University, University Park, Pennsylvania 16802, USA*
[3]*School of Engineering, Department of Physics, Center for Fluid Mechanics, and Brown Center for Theoretical Physics,
Brown University, Box D, Providence, Rhode Island 02912, USA*

Bacteria thrive in anisotropic media such as biofilms, biopolymer solutions, and soil pores. In strongly mechanically anisotropic media, physical interactions force bacteria to swim along a preferred direction rather than to execute the three-dimensional random walk due to their run-and-tumble behavior. Despite their ubiquity in nature and importance for human health, there is little understanding of bacterial mechanisms to navigate these media while constrained to one-dimensional motion. Using a biocompatible liquid crystal, we discovered two mechanisms used by *Bacillus subtilis* bacteria to switch directions in anisotropic media. First, the flagella assemble in bundles that work against each other from opposite ends of the cell body, and the dominating side in this flagellar "Tug-of-Oars" propels the bacterium along the nematic direction. Bacteria frequently revert their swimming direction 180° by a mechanism of flagellar buckling and reorganization on the opposite side of the cell. The Frank elastic energies of the liquid crystal dictate the minimum compression for the Euler buckling of a flagellum. Beyond a critical elasticity of the medium, flagellar motors cannot generate the necessary torque for flagellar buckling, and bacteria are stuck in their configuration. However, we found that bacteria can still switch swimming directions using a second mechanism where individual bundles alternate their rotation. Our results shed light on bacterial strategies to navigate anisotropic media and give rise to questions about sensing environmental cues and adapting at the level of flagellar bundles. The two adaptation mechanisms found here support the use of biocompatible liquid crystals as a synthetic model for bacterial natural environments.

I. INTRODUCTION

Run-and-tumble motion, i.e., abrupt alternations between directed swimming and random reorientations, is the most prolific feature of bacterial navigation in isotropic fluids like water [1–3]. However, bacteria thrive in non-Newtonian anisotropic environments. In the biofilms of several bacterial species, including *Escherichia coli*, *Vibrio cholerae*, and *Pseudomonas aeruginosa*, directional cell division and flagellar orientation lead to anisotropic growth [4,5], sculpting the complex surface patterns of the biofilms [6] and determining the organization of multicellular microbe communities [7]. In mechanically anisotropic fluids, where properties depend on the direction, hydrodynamic and steric interactions force bacteria to swim along a preferential path [8–14]. This mechanism constrains bacterial trajectories to the shear direction in mucus [14], which could be crucial in understanding the organization of microbiomes and the mechanics of bacterial colonization. Despite the prevalence of such anisotropic

biological media, it is unclear how the environment affects bacterial motility and their ability to find nutrients while exploring the space in a one-dimensional path instead of the three-dimensional (3D) run-and-tumble chemotaxis.

Here we study bacterial navigation of anisotropic media using a biocompatible liquid crystal amenable to effective computational modeling and reproducible experiments. The properties of lyotropic (water-based) disodium cromoglycate (DSCG) can be tuned to recreate typical isotropic environments where all directions have the same material properties, as well as an anisotropic medium where bacterial trajectories have long-range organization [11,15]. In waterlike solvents, DSCG molecules assemble into nanometer-sized stacks. These stacks are short and disorganized at low concentrations, forming isotropic suspensions. However, they can align parallel beyond a critical concentration, generating a nematic phase assembly [16]. Bacteria swim in nematic DSCG following unidirectional paths along the local director instead of the 3D random walk typically observed in isotropic suspensions [10,11]. Recent observations have shown that *E. coli* buckle and temporarily extend their flagella to the front of the cell in a frustrated attempt to tumble [17].

Here we examine the dynamics of *Bacillus subtilis* flagella in DSCG to quantitatively address the role of a fluid's anisotropic properties on bacterial navigation. We found that in Newtonian isotropic media, where cell bodies can freely rotate in 3D space, bacteria organize their flagellar bundles in

*Contact author: nuris.figueroa@colorado.edu

a V-shape configuration opposite the direction of motion. This angle becomes sharper as a function of solute concentration and its viscosity. In the nematic phase, we observed that flagellar bundles could have two possible configurations: a tightly packed tail behind the cell body or two small tails on opposite ends of the cell body, which we call Tug-of-Oars. We observed that tumbling attempts are responsible for a dynamic change in the number of flagella on opposite sides, which can reshape the tail configuration between one tail or two opposing tails and even invert the swimming direction. Higher liquid crystal (LC) concentration decreases the frequency of effective tumbles that change tail configurations, which we explain as a shift in the torque needed to buckle individual flagella in nematic LC. A minimum torque threshold for buckling also explains why high LC concentration and Frank elasticity suppress flagellar reorganization. In this regime, we identified a new mechanism for bacterial exploration of anisotropic media: Bacteria flip swimming directions by dynamically turning on and off individual entire bundles on opposite sides of the cell body. Our findings raise questions about the chemical and mechanical cues that govern the operation of flagellar bundles at high-viscosity loads.

II. RESULTS AND DISCUSSION

A. Flagellar configuration in nematic liquid crystals

We investigated the effect of liquid crystal concentration on the organization of flagellar bundles in *B. subtilis* bacteria. We studied suspensions of bacteria with stained and nonstained flagella in solutions of DSCG and, for comparison, a Newtonian suspension of polyvinylpyrrolidone (PVP40) (average molecular weight 40 kDa), dissolved in motility buffer (MB), which is a minimal medium where bacteria can swim but not divide. To observe the flagella, we labeled the flagellin protein (hag) of strain DS1919 with the fluorescent dye Alexa Fluor 488 (see Sec. IV for details). Our experiments span the entire concentration range of DSCG (0–19 wt. %) and PVP40 (0–25 wt. %), where bacteria can swim. We performed experiments under two different settings: (i) observation of individual bacteria with stained flagella in chambers made with untreated glass and (ii) long-time tracking of nonstained bacteria in a commercial treated glass chamber that aligns DSCG. The treated cells use established technology based on rubbed polymer surfaces to align LC [18,19]. The nematic field in untreated glass is uniform over scales of hundreds of microns, while in treated glass, the alignment spans a few millimeters (Fig. S2). The measurement chamber comprised two glass slides separated by a 10-µm-thick spacer in both cases.

In the isotropic (disordered) phase of DSCG, at concentrations roughly below 10 wt. % at 26 °C, bacterial flagella predominantly assemble into bundles in a V-shape configuration behind the cell body. This configuration has been observed before [20] and possibly results from the abundant flagella (26 ± 6), which cannot be accommodated into a single bundle around the elongated cell body (2–6 µm long [21]) due to geometrical factors [22], including the ratios of the body length to the length and pitch of the flagella (10 and 2.5 µm, respectively [23]), and the flagellar position on the body. Here we found that the average spread between

the bundles decreases with increasing DSCG concentration [Fig. 1(a)]. Eventually, either the flagella form a single bundle or the spread between bundles shrinks below the diameter of the cell body, resulting in an inversion of the V configuration. Since the angular vertex has shifted from the cell body to the free end of the flagella, we report these measurements with a negative sign. At higher DSCG concentrations, the negative angle reaches an asymptotic value of approximately $12°$. A theoretical estimate for the smallest possible arc is $2/8$ rad ($\sim 14°$), obtained for tight 8-µm-long flagella behind a cell body of diameter approximately 2 µm. The same phenomenon occurs for bacteria swimming in suspensions of PVP40, which are isotropic and Newtonian for the concentration range studied here. Our experiments show that the medium's elasticity or anisotropy is not responsible for the sharpening of the flagellar bundle. Understanding the relation between the angle and the fluid properties requires additional experiments and the development of a mathematical model of the flagellar hydrodynamic interactions with other flagella and steric interactions with the cell body. We expect that the bundle angle affects the bacterial speed, as a sharper bundle will have a higher swimming efficiency.

The organization of bacterial flagella in nematic DSCG is dramatically different from the isotropic phase [Figs. 1(a) and 1(b)]. In nematic DSCG (12–18.75 wt. %), we discovered that flagella can form two opposing tails, with bundles on both ends of the cell body. We call this swimming mode Tug-of-Oars since the two tails can propel the bacterium in opposite directions, akin to the motion of a boat in a Tug-of-Oars contest. Despite having close to 26 flagella scattered over their cell body, peritrichous *B. subtilis* bacteria in Tug-of-Oars resemble amphitrichous bacteria, such as *Magnetospirillum magneticum* or *Pseudomonas putida*, which have only two flagella located on opposite ends of the body. This mode exclusively arises in the nematic phase: *B. subtilis* flagella in isotropic PVP40 suspensions at similar viscosities form the negative V-shape configuration.

B. subtilis speeds are higher in DSCG than in isotropic PVP40 at the same viscosity [Fig. 1(c)]. Here we refer to the viscosity of DSCG along the nematic direction measured via microrheology [25]. Accordingly, bacteria can swim at high viscosities in nematic DSCG (approximately 250 cP) while they stall at approximately 50 cP in Newtonian PVP40. A possible explanation is the smaller wobbling angle of swimming cells in colloidal and polymeric suspensions, which can lead to up to 80% enhancement of bacterial motility [26–28]. Bacteria may experience lower effective viscosity due to shear-thinning effects or local shear melting of DSCG [11,29]. Furthermore, DSCG elasticity and quasi-one-dimensional signature of the bacterium-generated flow in nematic environments also lead to the swimming speed enhancement [15].

We found that the Tug-of-Oars in anisotropic media arises from tumbling attempts during constrained one-dimensional motion. This agrees with observations of *E. coli* flagellar reconfiguration during frustrated tumbles [17]. We compared flagellar alignments of the wild-type (run-and-tumble) strain with nontumbling *B. subtilis* (DK2178) in nematic DSCG. This strain retains the *hag* gene modification required to stain flagellin but lacks the chemotaxis gene *cheB* necessary for tumbling. Most nontumbling swimmers exclusively form a
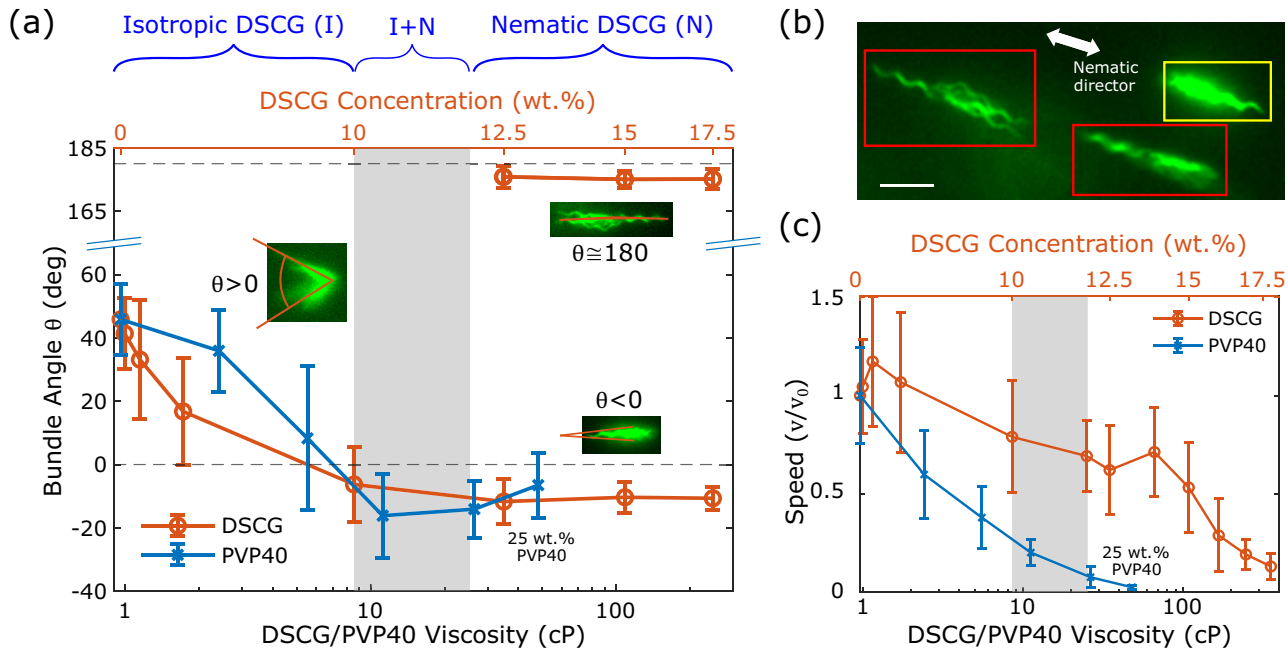
FIG. 1. Formation of the Tug-of-Oars configuration in anisotropic media. (a) Variation of bundle angle with DSCG and PVP40 concentration. Insets show examples of flagellar configurations in different regimes. The top axis indicates the concentration-dependent phase behavior for the DSCG solutions. Note that the PVP40 solutions are isotropic at all concentrations. Bacteria can organize their flagella into two tails exclusively in the nematic phase of DSCG, as indicated by the nearly 180° bundle angle. Each data point represents data from 20 bacteria and error bars denote standard deviations. (b) Bacteria swimming along the nematic director in nematic phase DSCG with one and two tails. Yellow and red boxes denote single- and double-tailed configurations, respectively. The scale bar is 5 μm. See also Movie S1. (c) Normalized average velocity of bacteria in DSCG and PVP40 for different viscosities. The normalization factor v_0 is the average speed in the motility buffer. Each data point represents data from average speeds of more than 100 bacteria (exact number in Table 1 in the Supplemental Material [24]) and error bars denote standard deviations. For an emphasis on the 0–50 cP regime, refer to Fig. S1.

single tightly packed bundle behind the cell body. On average, around three-quarters of wild-type bacteria (77%) swim with Tug-of-Oars at a given instant, contrasting with just 7% for the nontumbling swimmers (Fig. S3). The few exceptions in Tug-of-Oars likely originated during the initial conditions of the experiment while vortexing the solution or loading the measurement chamber.

B. Flagellar reconfiguration during restricted one-dimensional motion

In nematic DSCG, we observed that *B. subtilis* could dynamically change the flagellar balance on both ends of the cell, including a reversal from Tug-of-Oars to the negative V-shape configuration and vice versa. In all instances, flagella changed sides by buckling instead of swinging around to the opposite side of the cell, minimizing the disruption of the nematic ordering, as illustrated in Fig. 2(a).

The buckling site originates at the base of the flagellum, where torque is maximum, and subsequently moves towards the end of the flagellum. Figure 2(b) illustrates a flagellum reorganization at 15 wt. % DSCG. As the motor counterrotates, the flagellum helix close to the body temporarily turns straight between 0.2 and 0.8 s as the bending site travels to the free end. Then the flagellum returns to its right-handed helix form (1 s). This observation is consistent with flagella undergoing mechanical transformations in response to the high torsional load in viscous media [30] and DSCG [17].

Flagellar reconfiguration often switches the dominant side in the Tug-of-Oars. Figure 2(c) shows an image sequence where flagella on the bigger tail disassemble from the bundle (0–3.2 s) and reorganize on the other side of the body (3.2–5.6 s). For a typical bacterium, this results in an alternating forward and backward motion in a unidirectional constrained environment [Fig. 2(d)]. To quantify the rate of direction reversal, we defined a "flip" as an event in which the bacterium reverses its direction and swims in the new direction for at least 1 s. This period is much lower than the average time interval between flips at any DSCG concentration. We found that a time-based cutoff for flips is more robust than a cutoff based on the speed or the distance after reversing, which might introduce a secondary dependence on the properties of the solution. The flipping frequency as a function of DSCG concentration, shown in Fig. 2(e), shows a tenfold decrease from 30.5 mHz at 12.5 wt. % to 2.9 mHz at 18.75 wt. %. Thus, higher DSCG concentrations reduce the rate of flagellar exchange between opposing tails and the frequency of direction reversals (see Movie S4).

One possible explanation for the decreasing flipping frequency is the decreased rate of tumble events at higher DSCG concentrations. We discarded this hypothesis by measuring the frequency of tumble attempts in nematic DSCG. Since bacteria do not turn in 3D space in anisotropic environments, we defined a criterion based on the linear speeds of bacteria (Fig. S4). We performed a sensitivity analysis of our tumble classification method to ensure our results are robust up to
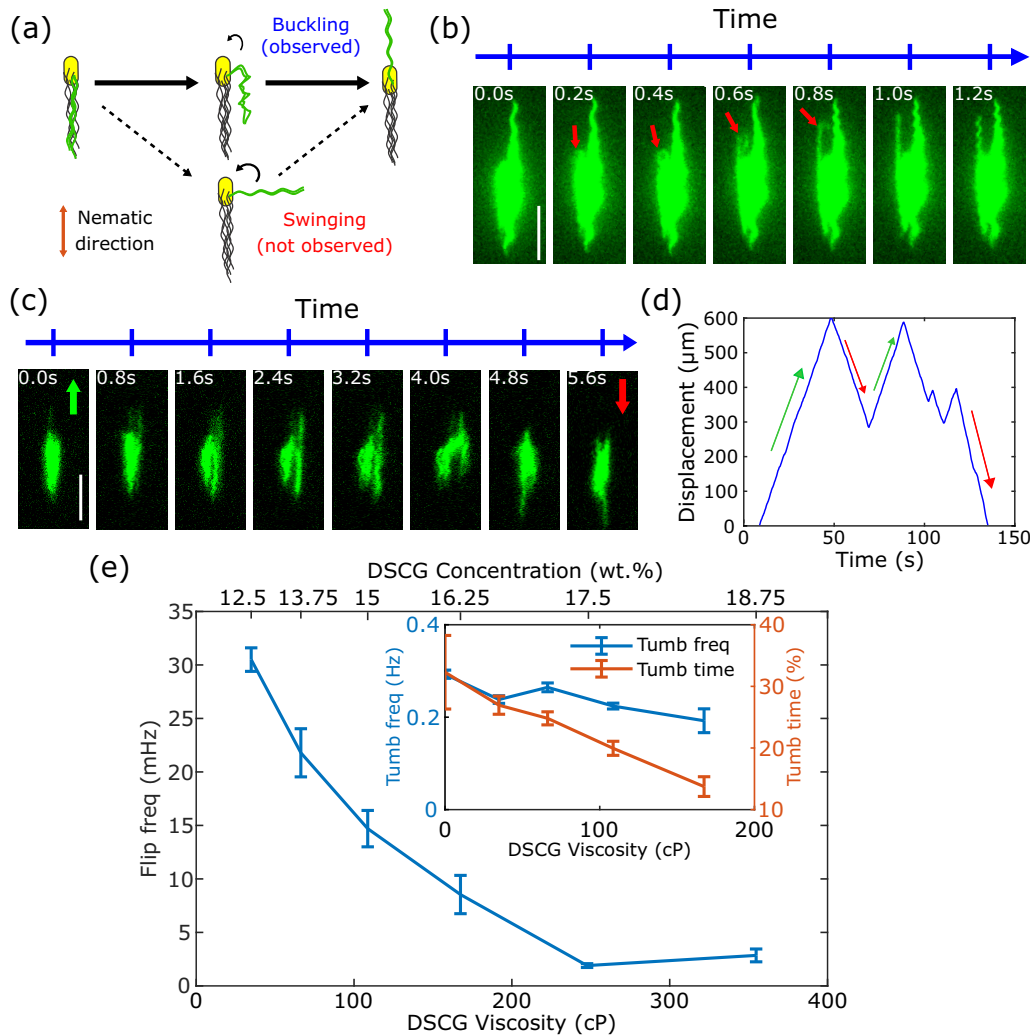
FIG. 2. Flagellar transfer between opposing sides in the Tug-of-Oars configuration. (a) Illustration of swinging and buckling mechanisms for flagella transferring between opposing tails. The green color indicates the flagella switching sides. Experiments only show the mechanism via flagella buckling, possibly because the swinging mechanism distorts DSCG stacks over a larger region. (b) Flagellum reorganizing between opposite sides via buckling at 15 wt. % DSCG. The red arrow shows the buckling site in the first four frames (0.0–0.6 s). The flagellum transforms between straight and helical forms between 0.8 and 1 s. The scale bar is 5 μm. See also Movie S3. (c) Sequence of snapshots displaying a bacterium transferring flagella between opposite ends to reverse directions. Flagella buckle at roughly 4 s. The scale bar is 5 μm. See also Movie S2. (d) Variation of displacement vs time for a bacterium in nematic DSCG. (e) Flipping frequency of bacteria as a function of DSCG viscosity. The inset shows the tumbling frequency and tumbling time of bacteria in DSCG. Tumbling time is calculated as a percentage of total trajectory time. Each data point represents data from more than 100 bacteria and error bars denote standard deviations.

16.25 wt. % DSCG (Fig. S5). Beyond this concentration, bacterial speeds become too low and the fluctuations too high to determine tumbles accurately using this method. The average frequency of tumble attempts is nearly constant across DSCG concentrations (approximately 250 mHz, or a corresponding period of approximately 4 s), in good agreement with our MB measurements and previous measurements in isotropic media [31,32].

The second and more likely hypothesis for the decrease in flipping frequency relies on the reduced rate of flagellar reorganization at higher DSCG concentrations. While tumbling rates remain constant, bacteria spend less time tumbling at increasing DSCG concentrations [Fig. 2(e) inset]. This observation contrasts with previous studies in viscous fluids reporting that the time required for flagella to unbundle in-

creased with increasing viscosity [33]. With increasing DSCG concentration, bundles are more tightly packed, requiring additional power to open the bundles within a tail.

C. Buckling model for flagellar rearrangement in nematic DSCG

To understand the decreasing flipping rates of flagellar filaments with increasing DSCG concentration, we developed a model that relates the probability of buckling to the elastic properties of the liquid crystal. For context, we start with a straight filament embedded in an elastic medium, similar to the analysis in Ref. [34]. A restoring force per unit length acts on the filament with a magnitude proportional to its transverse displacement. For small defections $x(z)$, the governing

equation for the filament centerline is

$$Ax_{zzzz} + Tx_{zz} + kx = 0, \qquad (1)$$

where A is the bending stiffness of the filament, T is the uniform (z-independent) compression force along the axis $\hat{z}$ of the filament, the subscript z denotes differentiation with respect to z, and k is the effective Hooke's law constant for the elastic medium [35]. Assuming a filament of length L with hinged ends, the solution for the above equation is $x = C \sin(n\pi z/L)$ when $T = T_{\text{cr}}$, with [35]

$$T_{\text{cr}} = \frac{\pi^2 A}{L^2} \left(n^2 + \frac{kL^4}{n^2 \pi^4 A} \right). \qquad (2)$$

Note that this equilibrium analysis only yields the value of the critical compression force. A more complete calculation of the growth rate of the instability would include a term representing the hydrodynamic drag of the medium on the filament, but the growth rate is not needed for our argument.

In a nematic liquid crystal, there is an elastic free-energy cost F whenever the director is nonuniform: $F = (K/2) \int \mathrm{d}^3 x (\partial_\alpha n_\beta)^2$, where K is the Frank modulus in the one-coupling-constant approximation, $\partial_\alpha = \partial/\partial x_\alpha$ is the derivative with respect the αth coordinate, and $\hat{\mathbf{n}}$ is the director [35]. Assuming the directors tend to align parallel to the filament tangent vector, we can model a filament in a nematic medium by supposing a restoring *torque* per unit length [35–37]

$$\mathbf{m} = -\beta K (\hat{\mathbf{t}} \cdot \hat{\mathbf{n}})(\hat{\mathbf{n}} \times \hat{\mathbf{t}}) \qquad (3)$$

acts when the filament's tangent vector $\hat{\mathbf{t}}$ rotates away from the alignment direction $\hat{\mathbf{n}} = \hat{\mathbf{z}}$ of the nematic. In this approximation, we treat the nematic as frozen and not responding to the deformation of the filament. Here β is a positive dimensionless constant. Thus, the torque balance on the filament is

$$Ax_{zzzz} + (T - \beta K)x_{zz} = 0. \qquad (4)$$

For hinged ends, the mode $x = C \sin(n\pi z/L)$ becomes unstable when $T > T_{\text{cr}}$, with

$$T_{\text{cr}} = \frac{n^2 \pi^2 A}{L^2} + \beta K. \qquad (5)$$

The primary effect of a nematic environment is shifting the critical compression to higher values. In reality, the compression does not come from point forces on each end of the filament but instead from the thrust force, which is distributed all along the flagellar filament, and from the force at the point of attachment of the filament to the motor, which ultimately arises from the drag of the cell body (see, e.g., [38,39]). Whether we assume hinged boundary conditions or more realistic but more complicated mixed boundary conditions at each end of the flagellar filament, our simplified model should give the same order of magnitude for the critical compression force in the real situation.

Adding the Frank constant term significantly affects the buckling criterion in DSCG. Recent measurements of the deformation of *B. subtilis* flagellar filaments via flow suggest $A \approx 2.4$ pN μm^2, implying that for a typical filament of length $L \approx 8$ μm the term $\frac{n^2 \pi^2 A}{L^2} \approx 0.38$ pN for the first bending mode [23]. Since the one coupling constant approximation is not

fully valid for DSCG, we used the average Frank constant for the splay, twist, and bend deformations using measurements from [40]. Substituting this value for DSCG ($K \approx 3$–30 pN) and taking $\beta \approx 1$, we find that $\beta K \gg \frac{n^2 \pi^2 A}{L^2}$. Thus, critical compression for buckling is simply

$$T_{\text{cr}} \approx K \qquad (6)$$

for a flagellar filament in nematic DSCG.

We now discuss how this changes the flipping frequency. The probability of having a flip $P_{\text{flip}}(t, t + \Delta t)$ within the interval $(t, t + \Delta t)$ is equal to the probability of having a motor reversal in that interval $P_{\text{reversal}}(t, t + \Delta t)$ times the probability that such a reversal carries enough force to produce filament bucking $P_{T > T_{\text{cr}}}$:

$$P_{\text{flip}}(t, t + \Delta t) = P_{\text{reversal}}(t, t + \Delta t) \times P_{T > T_{\text{cr}}}. \qquad (7)$$

Let us suppose there is stochasticity in the force generated by the motor during counterrotation. This would be explained by having a random number of stators (torque-generating protein complexes) bound to the motor at the time of a counterrotation. The maximum number of stators is 10 and the minimum 0. Here we explore two different hypotheses for the statistics of bound stators.

Model A. Suppose the probability density function is flat, so the force on any motor counterrotation is equally probable between 0 and T_{max}, where T_{max} is 10 times the force of one stator ($T_{\text{max}} = 10T_1$) (details in Supplemental Material [24] and Fig. S6). Then $P_{T > T_{\text{cr}}} = 1 - \frac{T_{\text{cr}}}{T_{\text{max}}} = 1 - \frac{K}{T_{\text{max}}}$ and the flipping frequency F will decay linearly as the Frank elasticity increases,

$$F = F_0 \left(1 - \frac{K}{T_{\text{max}}} \right). \qquad (8)$$

Here F_0 is the flipping frequency in a nematic medium where all attempts to reverse can successfully buckle the flagella. Flips will be impossible for media where $K > T_{\text{max}}$. The linear fit in Fig. 3(a) only includes the first four experimental points for reasons explained in the next section. The fitting value $T_1 \approx 1.9$ pN is in agreement with the 1.1 pN estimated from a stall torque of 2200 pN nm for ten stators in [41] and filament radius of 200 nm.

Model B. Suppose the stators can independently bind to the motor in up to ten sites. The probability density function can be approximated as a Gaussian with mean $\mu = 5.0$ and standard deviation $\sigma = 1.62$ (details in the Supplemental Material [24] and Fig. S6). The frequency of flips decays as

$$F = F_0 \left[\frac{1}{2} - \frac{1}{2} \operatorname{erf} \left(\frac{K - \mu T_1}{\sigma T_1 \sqrt{2}} \right) \right] \qquad (9)$$

[Fig. 3(a)], with fitting value $T_1 \approx 2.38$ pN.

The above models A and B do not consider variation in the number of stators across DSCG concentration. The frictional drag acting on bacteria in concentrated DSCG can be estimated using Stokes' law as $F_{\text{drag}} \approx 6\pi \eta r v$, where η is the viscosity, r is the cell radius, and v is the bacterium's speed. Beyond 13.75 wt. % DSCG concentration, the viscous drag
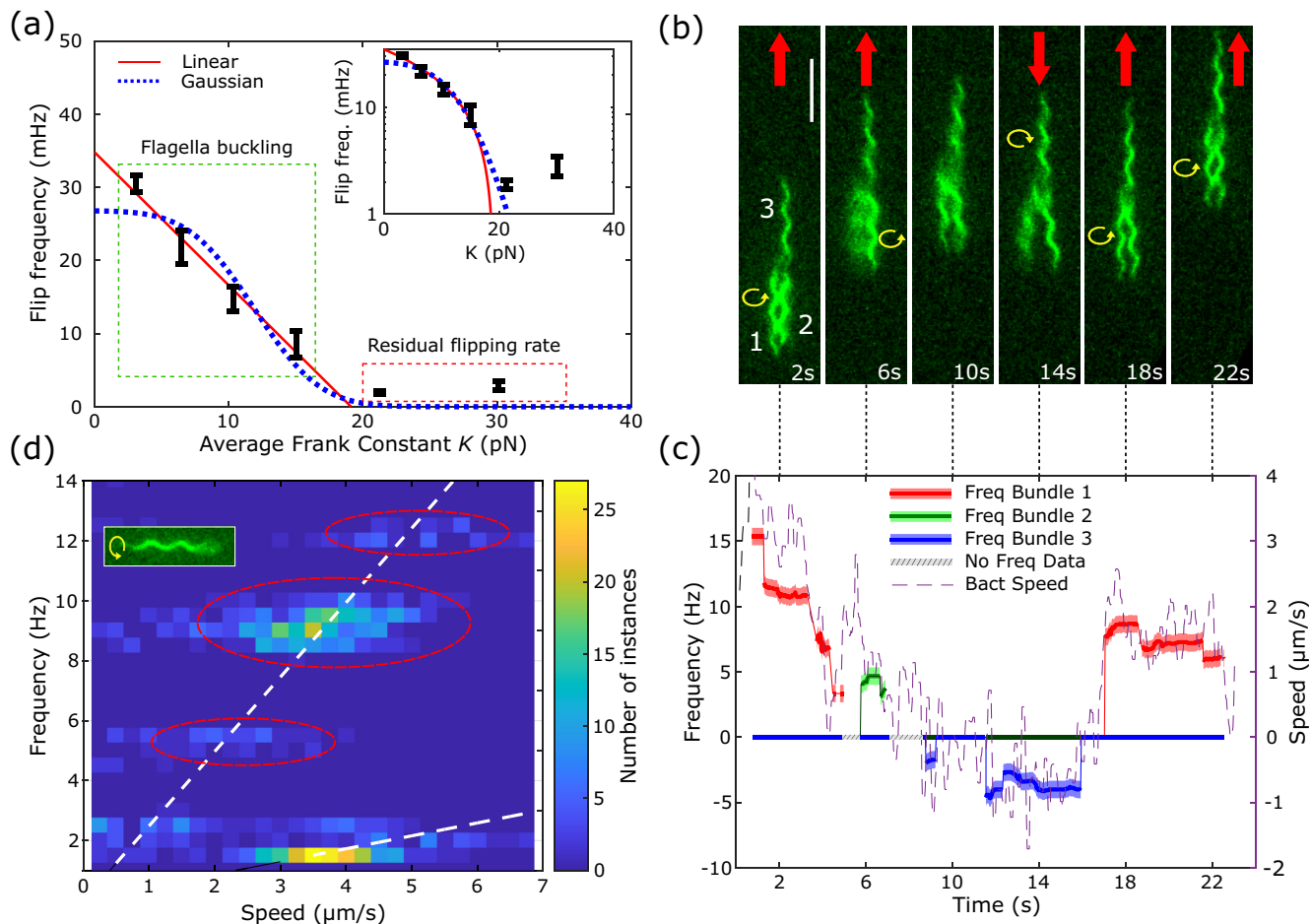
FIG. 3. Mechanism for direction reversal at high DSCG concentrations. (a) Variation of flipping frequency as a function of average Frank constant of DSCG. The red solid line and blue dashed line show fits for experimental data using models A [Eq. (8)] and B [Eq. (9)], respectively. The green box indicates the regime that can be explained by our modeling, while the red box indicates a regime with residual flipping rates. The inset shows the same plot on a semilogarithmic scale. (b) Bacterium with three flagellar bundles swimming in 18.75% DSCG. The first panel in the time series shows bundles 1 and 2 on one end and bundle 3 on the opposite end. The scale bar is 5 μm. (c) Plot of the frequency of rotating bundles and speed for the bacterium corresponding to the time series B. The frequency of bundle 3 is shown with a negative sign. No frequency data were obtained for intervals when the moving bundle was out of focus or blocked by a stationary bundle. See also Movie S5. (d) Density plot of speed and frequencies of bundle rotation for a bacterium with a single bundle in 18.75% DSCG (bacterium in inset). The fast Fourier transform of the rotating bundle shows discrete regimes of rotation frequencies. See also Movie S5.

remains constant [approximately 18 pN (Fig. S7)]; therefore, we think the cells are delivering their maximum power.

D. Second mechanism for navigating highly anisotropic environments

Bacteria can generate enough force to buckle their flagella only if that force is bigger than the Frank elasticity of the medium [Eq. (6)]. The estimated maximum force of 18 pN corresponds to a concentration of 17.3 wt. %. Despite this, some bacteria can reverse directions up to $K \sim 30$ pN. We called this *residual flipping rate* in Fig. 3(a).

We found that bacteria stuck in the Tug-of-Oars mode during initial conditions can reverse directions by activating or deactivating individual bundles on opposite sides of the body. For example, the bacterium shown in Fig. 3(b) has three distinct flagellar bundles: Bundles 1 and 2 are on the bottom and bundle 3 is on the top. The bacterium of Fig. 3(b) was

propelled solely by bundle 1 from 0 to 5 s (bottom of panel). Between 5 and 8 s, bundle 1 stops and bundle 2 takes over to keep pushing the bacterium "up," represented by a red arrow at the top of the panel. Bundle 3 drives the bacterium "down" between 12 and 16 s. At this point, bundle 1 alone pushes the bacterium up, resulting in a second flip. The active bundle frequency changes in time and stays proportional to the bacterium speed, which is noisier and represented on the right *y* axis. This mechanism is responsible for nonzero flipping rates, even at high Frank energies where flagellar buckling and reorganization are unfeasible.

The frequency of individual bundles in Fig. 3(c) can be interpreted as discrete, with periods of constant frequency followed by abrupt changes in frequency. The flagellar frequency was determined by tracking the position of several points on the flagella, transforming to Fourier space, and summing over to average out the noise (Fig. S8). A similar analysis on a single-tailed bacterium over a longer period

without flips clearly shows discretized frequencies of flagellar rotation [Fig. 3(d)] on three regions highlighted with red ovals around 4–6, 8–10, and 12–13 Hz. These frequencies are in good agreement with previous measurements in liquid crystals, corresponding to roughly 1–2 Hz (body rotation) and 8–10 Hz (flagellar rotation) [11].

In *E. coli*, discrete changes in the frequency of individual flagella have been associated with variation in the number of stators per flagella as a response to mechanical load [42–47]. However, while *E. coli* and *B. subtilis* share the fundamental architecture and function of their flagellar motors, differences exist in the composition, energy source utilization, rotational dynamics, and chemotaxis signaling [48]. Wild-type *B. subtilis* can assemble two types of stator proteins MotAB and MotPS to power the flagellar filaments. In isotropic and homogenous environments, MotAB is the dominant stator unit that uses proton motive force to rotate the flagellum. However, in viscous environments with high sodium ion concentrations (approximately 200 mM Na^+), MotPS proteins can bind to rotors and generate sodium motive force for flagellar rotation [41,49]. Biological fluids like blood and mucus have enough sodium ion content (approximately 170 mM) [50] to support sodium motive force through MotPS. MotPS might be essential in rotating flagella in our experiments since the ionization of DSCG in water generates a high sodium ion external environment (approximately 700 mM Na^+ for 15 wt. %). The interplay between MotAB and MotPS will govern the rotation frequency of a flagellar bundle at high DSCG concentrations. However, our experiments cannot identify the molecular mechanism responsible for the discrete torque on the flagella or the dynamic switching on and off of bundles observed here. Labeling and tracking stators within the cell could provide clues to the origin of these phenomena.

In addition, our experiments focus on bundles composed of several flagella, and additional factors could be at play. As the nematic environment hinders the movement of flagella around the cell, restricted winding and unwinding of bundles may lead to intertwining flagellar configurations that interfere with rotation by creating intermittent jamming of individual bundles or modifying the resistance to rotation in bundles. These are factors that smear out the frequency discreteness.

III. CONCLUSIONS

We have observed a novel adaptation by peritrichous bacteria into a double-polar flagellar bundle configuration to navigate anisotropic media. This adaptation allows bacteria to reverse the direction of motion when the restrictive medium hinders the 3D rotation of the cell body. The main finding is that *Bacillus subtilis* bacteria can reverse the swimming direction by two complimentary mechanisms. At low elastic (Frank) energy of the nematic medium, bacteria can rearrange flagella between opposing tails via polymorphic transformations during events of motor counterrotation along the trajectory. To buckle the flagellum, the motor must generate a critical torque proportional to the Frank energy of the medium. Thus, the frequency of flagellar rearrangement and velocity reversals decrease with DSCG concentration until Frank energy reaches a critical threshold. Beyond this

point, bacteria can only reverse directions by selectively using flagellar bundles on opposing ends of their body. Adaptation to the Tug-of-Oars configuration allow bacteria to explore highly anisotropic media and perhaps also extremely narrow channels.

The fact that bacteria have evolved at least two mechanisms to navigate mechanically anisotropic media suggests that they may be using these mechanisms in their natural environment, which can be modeled by the biocompatible liquid crystal DSCG. The DSCG represents a synthetic model to study bacterial transport in mucus, which can be highly anisotropic [14,51–55] and has enormous importance in the organization of microbiomes and protection against pathogens inside our organisms.

IV. METHODS

A. Microscopy

An Olympus IX-83 inverted microscope was used for bacteria visualization in bright-field and fluorescence imaging. Bacteria locomotion videos were collected in $10/20/40/60\times$ for bright-field and $20/40/60\times$ for fluorescence imaging. Frame rates for data acquisition were 20–30 frames per second (bright field) and 5–30 frames per second (fluorescence). The Hamamatsu ORCA-Flash4.0 V3 camera was used with a resolution of 2048×2048 pixels.

B. Preparation and staining of bacterial cultures

The *B. subtilis* bacteria used for these experiments are a run-and-tumble strain (DS1919) and a nontumbling swimming strain (DK2178). Both strains were acquired from the Kearns Laboratory at Indiana University Bloomington. A colony of these bacteria was grown overnight from a Petri dish in liquid Luria-Bertani broth at $30\,^\circ$C until an optical density of approximately 0.6–1.0 was reached. 1.5 ml of bacteria in the liquid medium were centrifuged at 4000 rpm for 3 min. The supernatant was removed, and the bacteria were resuspended in 100 μm of phosphate buffer solution (PBS). This solution was mixed with 1 μl of 2.5 μg/μl Alexa Fluor 488, a green dye with an excitation peak at 488 nm and an emission peak at 496 nm. After waiting for 5 min to let the dye disperse, the bacteria were washed twice in 1.5 ml of PBS to remove the excess dye. Finally, the bacteria were resuspended in 1.5 ml of motility buffer (MB composition: 0.1 mM EDTA, 1 μM l-methionine, 10 mM sodium lactate, 6.2 mM K_2HPO_4, 3.9 mM KH_2PO_4). For measurements on bacteria motility and flagellar orientation, the bacterial solution was further diluted 1:100 in the respective % w/v ratio solution of DSCG and PVP40 in MB and mixed in a vortex mixer. To observe flagella without impacting the swimming ability of bacteria, we shined periodic low-intensity bursts of blue light on the microchamber.

C. Bacteria in DSCG and PVP40 solutions

DSCG solutions were prepared by mixing DSCG (TCI Chemicals) with MB, heating, and sonicating the sample until complete dissolution. Similarly, PVP40 solutions were made by mixing the powder with MB and sonicating until

complete dissolution. The bulk viscosity of isotropic solutions was measured using a rheometer (Anton Parr). For nematic phase DSCG, we used microrheology data to get viscosity along the nematic direction [25].

D. Chamber preparation

Custom chambers for observing stained flagella were prepared by attaching two 0.17-mm glass slides with a 10-µm spacer purchased from Nitto Denko Corp. Bacterial solutions were inserted via a narrow gap in the spacer. Commercial chambers with inner surfaces coated with polyimide were purchased from Instec Inc. for long-time tracking of nonstained bacteria.

All images were processed via custom scripts in MATLAB, using the Image Processing Toolbox and Curve Fitting Toolbox.

[1] H. C. Berg and D. A. Brown, Chemotaxis in *Escherichia coli* analysed by three-dimensional tracking, Nature (London) **239**, 500 (1972).

[2] N. Figueroa-Morales, R. Soto, G. Junot, T. Darnige, C. Douarche, V. A. Martinez, A. Lindner, and É. Clément, 3D Spatial exploration by *E. coli* echoes motor temporal variability, Phys. Rev. X **10**, 021004 (2020).

[3] K. Taute, S. Gude, S. Tans, and T. Shimizu, High-throughput 3D tracking of bacteria on a standard phase contrast microscope, Nat. Commun. **6**, 8776 (2015).

[4] A. Van Wey, A. Cookson, T. Soboleva, N. Roy, W. McNabb, A. Bridier, R. Briandet, and P. Shorten, Anisotropic nutrient transport in three-dimensional single species bacterial biofilms, Biotechnol. Bioeng. **109**, 1280 (2012).

[5] D. O. Serra, A. M. Richter, G. Klauck, F. Mika, and R. Hengge, Microanatomy at cellular resolution and spatial order of physiological differentiation in a bacterial biofilm, mBio **4**, 10 (2013).

[6] C. Zhang, B. Li, X. Huang, Y. Ni, and X.-Q. Feng, Morphomechanics of bacterial biofilms undergoing anisotropic differential growth, Appl. Phys. Lett. **109**, 143701 (2016).

[7] B. Maier, How physical interactions shape bacterial biofilms, Annu. Rev. Biophys. **50**, 401 (2021).

[8] I. S. Aranson, Bacterial active matter, Rep. Prog. Phys. **85**, 076601 (2022).

[9] P. C. Mushenheim, R. R. Trivedi, D. B. Weibel, and N. L. Abbott, Using liquid crystals to reveal how mechanical anisotropy changes interfacial behaviors of motile bacteria, Biophys. J. **107**, 255 (2014).

[10] P. C. Mushenheim, R. R. Trivedi, H. H. Tuson, D. B. Weibel, and N. L. Abbott, Dynamic self-assembly of motile bacteria in liquid crystals, Soft Matter **10**, 88 (2014).

[11] S. Zhou, A. Sokolov, O. D. Lavrentovich, and I. S. Aranson, Living liquid crystals, Proc. Natl. Acad. Sci. USA **111**, 1265 (2014).

[12] S. Zhou, O. Tovkach, D. Golovaty, A. Sokolov, I. S. Aranson, and O. D. Lavrentovich, Dynamic states of swimming bacteria in a nematic liquid crystal cell with homeotropic alignment, New J. Phys. **19**, 055006 (2017).

[13] M. M. Genkin, A. Sokolov, O. D. Lavrentovich, and I. S. Aranson, Topological defects in a living nematic ensnare swimming bacteria, Phys. Rev. X **7**, 011029 (2017).

[14] N. Figueroa-Morales, L. Dominguez-Rubio, T. L. Ott, and I. S. Aranson, Mechanical shear controls bacterial penetration in mucus, Sci. Rep. **9**, 9713 (2019).

[15] A. Sokolov, S. Zhou, O. D. Lavrentovich, and I. S. Aranson, Individual behavior and pairwise interactions between microswimmers in anisotropic liquid, Phys. Rev. E **91**, 013009 (2015).

[16] S. Zhou, *Lyotropic Chromonic Liquid Crystals: From Viscoelastic Properties to Living Liquid Crystals* (Springer, Cham, 2017), pp. 51–75.

[17] M. Goral, E. Clement, T. Darnige, T. Lopez-Leon, and A. Lindner, Frustrated 'run and tumble' of swimming *Escherichia coli* bacteria in nematic liquid crystals, Interface Focus **12**, 20220039 (2022).

[18] O. D. Lavrentovich and T. Ishikawa, Bulk alignment of lyotropic chromonic liquid crystals, U.S. Patent No. 6,411,354 (25 June 2002).

[19] J. Stöhr and M. Samant, Liquid crystal alignment by rubbed polymer surfaces: A microscopic bond orientation model, J. Electron Spectrosc. Relat. Phenom. **98-99**, 189 (1999).

[20] J. Najafi, M. R. Shaebani, T. John, F. Altegoer, G. Bange, and C. Wagner, Flagellar number governs bacterial spreading and transport efficiency, Sci. Adv. **4**, eaar6425 (2018).

[21] J. Errington and L. T. van der Aart, Microbe profile: *Bacillus subtilis*: model organism for cellular development, and industrial workhorse, Microbiology **166**, 425 (2020).

[22] J. Clopés and R. G. Winkler, Flagellar arrangements in elongated peritrichous bacteria: bundle formation and swimming properties, Eur. Phys. J. E **44**, 17 (2021).

[23] X. Shen, P. N. Tran, B. Z. Tay, and Marcos, Bending stiffness characterization of *Bacillus subtilis'* flagellar filament, Biophys. J. **121**, 1975 (2022).

[24] See Supplemental Material at http://link.aps.org/supplemental/10.1103/PRXLife.2.033004 for details.

[25] A. Habibi, C. Blanc, N. B. Mbarek, and T. Soltani, Passive and active microrheology of a lyotropic chromonic nematic liquid crystal disodium cromoglycate, J. Mol. Liq. **288**, 111027 (2019).

[26] S. Kamdar, S. Shin, P. Leishangthem, L. F. Francis, X. Xu, and X. Cheng, The colloidal nature of complex fluids enhances bacterial motility, Nature (London) **603**, 819 (2022).

[27] A. E. Patteson, A. Gopinath, M. Goulian, and P. E. Arratia, Running and tumbling with *E. coli* in polymeric solutions, Sci. Rep. **5**, 15761 (2015).

[28] E. Tamar, M. Koler, and A. Vaknin, The role of motility and chemotaxis in the bacterial colonization of protected surfaces, Sci. Rep. **6**, 19616 (2016).

[29] M. M. Genkin, A. Sokolov, and I. S. Aranson, Spontaneous topological charging of tactoids in a living nematic, New J. Phys. **20**, 043027 (2018).

[30] S. Mukherjee and D. B. Kearns, The structure and regulation of flagella in *Bacillus subtilis*, Annu. Rev. Genet. **48**, 319 (2014).

[31] M. Sidortsov, Y. Morgenstern, and A. Beér, Role of tumbling in bacterial swarming, Phys. Rev. E **96**, 022407 (2017).

[32] L. Turner, L. Ping, M. Neubauer, and H. C. Berg, Visualizing flagella while tracking bacteria, Biophys. J. **111**, 630 (2016).

[33] Z. Qu, F. Z. Temel, R. Henderikx, and K. S. Breuer, Changes in the flagellar bundling time account for variations in swimming behavior of flagellated bacteria in viscous media, Proc. Natl. Acad. Sci. USA **115**, 1707 (2018).

[34] Y. Guo, Y. Liu, J. X. Tang, and J. M. Valles, Jr., Polymerization force driven buckling of microtubule bundles determines the wavelength of patterns formed in tubulin solutions, Phys. Rev. Lett. **98**, 198103 (2007).

[35] L. D. Landau and E. M. Lifshitz, *Theory of Elasticity*, 3rd ed. (Pergamon, Oxford, 1986).

[36] F. Brochard and P.-G. de Gennes, Theory of magnetic suspensions in liquid crystals, J. Phys. France **31**, 691 (1970).

[37] N. Kikuchi, A. Ehrlicher, D. Koch, J. A. Käs, S. Ramaswamy, and M. Rao, Buckling, stiffening, and negative dissipation in the dynamics of a biopolymer in an active medium, Proc. Natl. Acad. Sci. USA **106**, 19776 (2009).

[38] M. Tournus, A. Kirshtein, L. Berlyand, and I. S. Aranson, Flexibility of bacterial flagella in external shear results in complex swimming trajectories, J. R. Soc. Interface **12**, 20140904 (2015).

[39] M. Potomkin, M. Tournus, L. Berlyand, and I. Aranson, Flagella bending affects macroscopic properties of bacterial suspensions, J. R. Soc. Interface **14**, 20161031 (2017).

[40] S. Zhou, K. Neupane, Y. A. Nastishin, A. R. Baldwin, S. V. Shiyanovskii, O. D. Lavrentovich, and S. Sprunt, Elasticity, viscosity, and orientational fluctuations of a lyotropic chromonic nematic liquid crystal disodium cromoglycate, Soft Matter **10**, 6571 (2014).

[41] N. Terahara, Y. Noguchi, S. Nakamura, N. Kami-ike, M. Ito, K. Namba, and T. Minamino, Load- and polysaccharide-dependent activation of the Na$^+$-type MotPS stator in the *Bacillus subtilis* flagellar motor, Sci. Rep. **7**, 46081 (2017).

[42] N. Wadhwa, R. Phillips, and H. C. Berg, Torque-dependent remodeling of the bacterial flagellar motor, Proc. Natl. Acad. Sci. USA **116**, 11764 (2019).

[43] N. Wadhwa, Y. Tu, and H. C. Berg, Mechanosensitive remodeling of the bacterial flagellar motor is independent of direction of rotation, Proc. Natl. Acad. Sci. USA **118**, e2024608118 (2021).

[44] N. Wadhwa, A. Sassi, H. C. Berg, and Y. Tu, A multi-state dynamic process confers mechano-adaptation to a biological nanomachine, Nat. Commun. **13**, 5327 (2022).

[45] A. L. Nord, E. Gachon, R. Perez-Carrasco, J. A. Nirody, A. Barducci, R. M. Berry, and F. Pedaci, Catch bond drives stator mechanosensitivity in the bacterial flagellar motor, Proc. Natl. Acad. Sci. USA **114**, 12952 (2017).

[46] H. Shi, S. Ma, R. Zhang, and J. Yuan, A hidden state in the turnover of a functioning membrane protein complex, Sci. Adv. **5**, eaau6885 (2019).

[47] Y. Niu, R. Zhang, and J. Yuan, Flagellar motors of swimming bacteria contain an incomplete set of stator units to ensure robust motility, Sci. Adv. **9**, eadi6724 (2023).

[48] C. V. Rao, J. R. Kirby, and A. P. Arkin, Design and diversity in bacterial chemotaxis: a comparative study in *Escherichia coli* and *Bacillus subtilis*, PLoS Biol. **2**, e49 (2004).

[49] M. Ito, D. B. Hicks, T. M. Henkin, A. A. Guffanti, B. D. Powers, L. Zvi, K. Uematsu, and T. A. Krulwich, MotPS is the stator-force generator for motility of alkaliphilic *Bacillus*, and its homologue is a second functional Mot in *Bacillus subtilis*, Mol. Microbiol. **53**, 1035 (2004).

[50] D. Song, E. Iverson, L. Kaler, S. Bader, M. A. Scull, and G. A. Duncan, Modeling airway dysfunction in asthma using synthetic mucus biomaterials, ACS Biomater. Sci. Eng. **7**, 2723 (2021).

[51] J. Perez-Vilar, Mucin granule intraluminal organization, Am. J. Respir. Cell Mol. Biol. **36**, 183 (2007).

[52] F. A. Bettelheim and S. K. Dey, Molecular parameters of submaxillary mucins, Arch. Biochem. Biophys. **109**, 259 (1965).

[53] W. Liao and I. S. Aranson, Viscoelasticity enhances collective motion of bacteria, PNAS Nexus **2**, pgad291 (2023).

[54] H. Chi, A. Gavrikov, L. Berlyand, and I. S. Aranson, Interaction of microswimmers in viscoelastic liquid crystals, Commun. Phys. **5**, 274 (2022).

[55] H. Chi, M. Potomkin, L. Zhang, L. Berlyand, and I. S. Aranson, Surface anchoring controls orientation of a microswimmer in nematic liquid crystal, Commun. Phys. **3**, 162 (2020).